nature portfolio

https://doi.org/10.1038/s41566-021-00906-8

Supplementary information

Two-step absorption instead of two-photon absorption in 3D nanoprinting

In the format provided by the authors and unedited

Two-step absorption instead of two-photon absorption in 3D nanoprinting

Supplementary Information

Vincent Hahn, Tobias Messer, N. Maximilian Bojanowski, Ernest Ronald Curticean, Irene Wacker, Rasmus R. Schröder, Eva Blasco, and Martin Wegener

Supplementary Notes

Energy-level model rate calculations

Fig. 2a shows a sketch of an energy-level model for two-step absorption, with ground state A, intermediate states B and B', and upper state C. We assume rapid nonradiative decay between B and B'. Radicals are rapidly generated from a population of energy level C, leading to the dose $D = [\mathrm{C}]$. The initial population at $t = 0$ is $[\mathrm{A}] = 1, [\mathrm{B}] = 0$, and $[\mathrm{C}] = 0$. Accordingly, the governing rate equations are

$$[\dot{\mathrm{A}}] = -k_1[\mathrm{A}] + k_\mathrm{D}[\mathrm{B}], \tag{1}$$

$$[\dot{\mathrm{B}}] = +k_1[\mathrm{A}] - k_\mathrm{D}[\mathrm{B}] - k_2[\mathrm{B}], \tag{2}$$

$$[\dot{\mathrm{C}}] = +k_2[\mathrm{B}], \tag{3}$$

with k_1 and k_2 being the transition rate coefficients from state A to state B and from state B to state C, respectively. Here, k_D is the intermediate-state B decay rate coefficient – the inverse of the intermediate state lifetime τ. This differential equation system is solved analytically using Mathematica to obtain explicit expressions for the functions $[\mathrm{A}](t)$, $[\mathrm{B}](t)$, and $[\mathrm{C}](t)$ (cf. Figs. 2b and 2c). The results shown Figs. 2d and 2e have been computed by numerical searches of zero crossings using Matlab.

Supplementary Figures

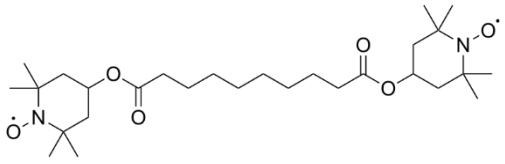

Fig. S1 | Chemical structure of bis(2,2,6,6-tetramethyl-4-piperidyl-1-oxyl) sebacate (BTPOS).

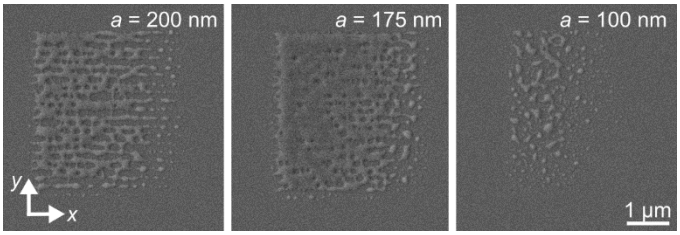

Fig. S2 | Scanning electron micrographs of 3D printed line gratings with different grating periods when omitting the quencher BTPOS in the photoresist PR1 containing benzil. The fast scanning direction is along the $-x$ direction, the slow scanning direction is along the $+y$ direction. The used laser powers are ~ 2 µW. All other 3D printing parameters are identical to the line gratings shown in Fig. 5 in the main paper. These results show, that the quencher is an essential ingredient in the studied photoresists for making two-step absorption a suitable excitation mechanism for 3D laser nanoprinting.

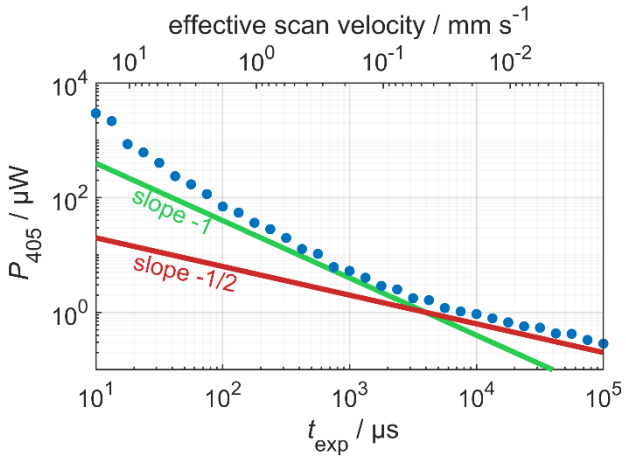

Fig. S3 | Laser power versus exposure time for the photoresist PR4, containing Irgacure 369 (50 mM) instead of benzil. The red and green straight lines are guides to the eye. For exposure times $t_{\mathrm{exp}} > 4$ ms, the data are consistent with a slope of $-1/2$. For exposure times $t_{\mathrm{exp}} < 100$ µs, the data indicate a slope close to -1.

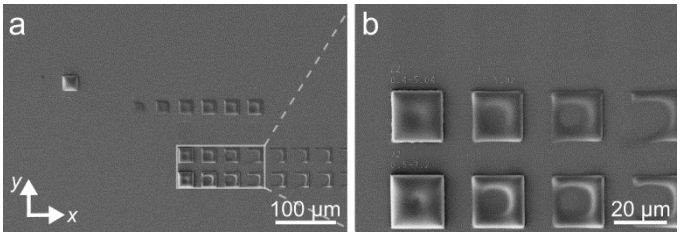

Fig. S4 | Top-view scanning electron micrograph of attempts to 3D print woodpile structures using the photoresist PR4, containing Irgacure 369 as photoinitiator. **a,** Overview image. The structures have been printed from top left to bottom right.

b, Zoom-in of panel a. The threshold dose increases in the proximity of previously 3D printed structures. These results show that 3D laser nanoprinting is essentially impossible when replacing benzil (supporting two-step absorption) by Irgacure 369 (supporting one-photon absorption) as photoinitiator.

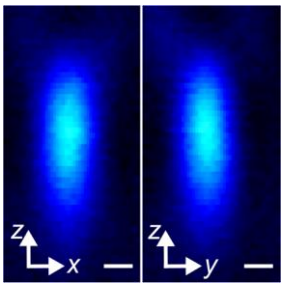

Fig. S5 | Laser focus measurement when immersing the objective lens using the dip-in photoresist PR2 instead of the objective lens immersion fluid. Scale bars $100\ \mathrm{nm}$.

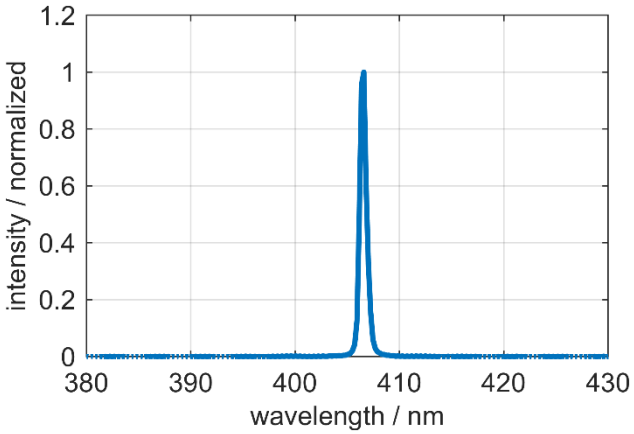

Fig. S6 | Spectrum of the laser diode emission at the operating temperature of $\boldsymbol{T_{\mathrm{Diode}} = 25°\mathrm{C}}$. The peak wavelength is at $\lambda_{\mathrm{P}} = 406.5\ \mathrm{nm}$, which is slightly red-shifted from the diode's nominal wavelength of $\lambda = 405\ \mathrm{nm}$.

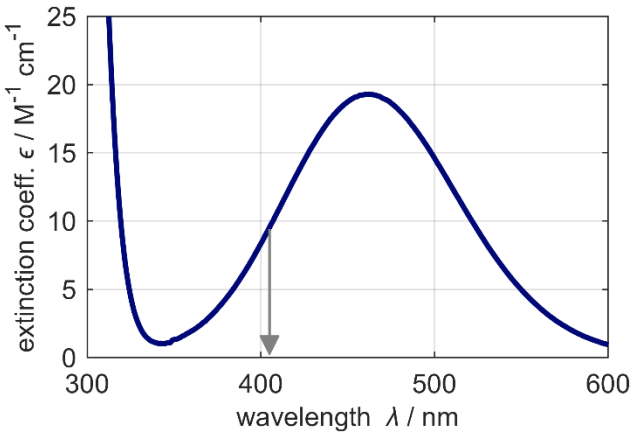

Fig. S7 | Ground-state extinction spectrum of BTPOS in acetonitrile. The gray arrow indicates the excitation wavelength.

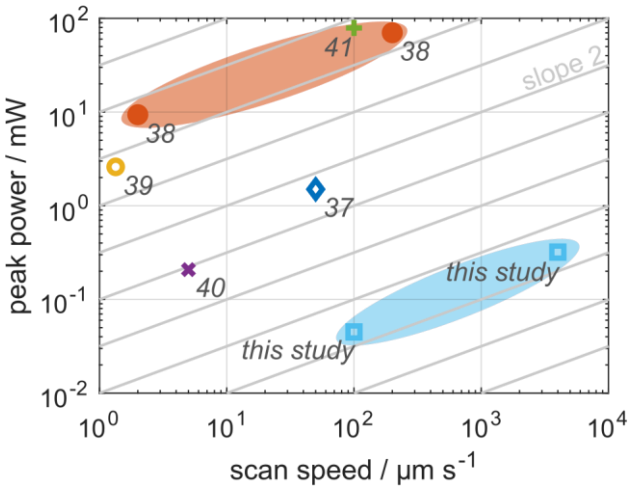

Fig. S8 | Overview of 3D laser polymer printing using (quasi-)continuous wave lasers. The numbers assigned to the symbols correspond to the references given in the main manuscript[37-41]. These references are plotted versus scan speed and laser peak power, respectively, on a double-logarithmic scale. It can be seen that two-step absorption (labelled as "this study") enables scan speeds that are up to three orders of magnitude faster than in previous studies, and (peak) laser powers that are up to three orders of magnitude lower. The gray straight lines with a slope of 2 are guides to the eye. Note that this overview does not include the achieved spatial resolution.

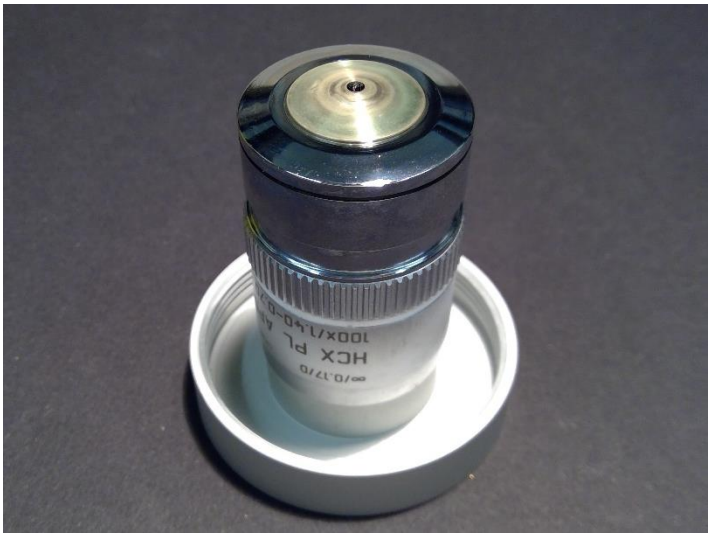

Fig. S9 | Photograph of the used microscope objective lens with applied photoresist for dip-in 3D laser nanoprinting. For dip-in 3D laser nanoprinting, the amount of applied photoresist is on the order of a few microliters. Therefore, the photoresist cannot be seen on this photograph. Note that the bronze colored disk on top of the microscope lens is not the photoresist, but part of the objective lens metallic body.

Supplementary Tables

Supplementary Table S1 | List of 3D printing parameters for all structures shown in the figures in the main paper. In the "Development" column, "CPD" stands for "Critical Point Drying".

	Hatching (nm)	Slicing (nm)	Laser Power (μW)	Scan Speed (mm/s)	Resist	Dip-In?	Development
5b	variable	-	66	0.1	PR1	no	acetone
5c	variable	variable	~45 (a=300 nm)	0.1	PR1	no	CPD
5d	(300)	(106)	As in 3c	0.1	PR1	no	CPD
6a	-	-	500	0.5	PR1	no	acetone
6b	30	100	320	1.0	PR1	no	acetone
6c	50	100	270	3.0	PR2	yes	acetone
6d	30	100	320	4.0	PR1	no	acetone
6e	50	100	400	1.0	PR3	no	acetone

Supplementary Methods

Reconstructing 3D models from the woodpile cross sections

The movie 3D_volume_reconstruction shows a 3D rendering of the volume of the woodpile structure (rod spacing $a = 300$ nm) reconstructed from a scanning electron microscope image after embedding and ultrathin sectioning (cf. Fig. 5e).

The 3D volume was reconstructed making use of the known periodicity of the laser written woodpile. The unit cell of that periodic structure is sampled in an approximate b-direction (corresponding to the x-coordinate in Fig. 5e) in 33 bins, which were obtained from the image of the section through the structure. The number of bins is determined by the tilting of the section relative to the ac lattice plane (denoted as yz in Fig. 5), which in this example was tilted by $1.7°$. The unit cell was filled with structural information by placing image data slice after slice in the cell under the correct Euler angles relative to the crystallographic axes a, b, c and at distances $b/33$. The data of each of these slices were obtained from image Fig. 5e, moving in unit cell steps along the approximate a axis (i.e. image coordinate y).

This procedure was automated using the image processing scripting software SPIDER[50] selecting the basic periodic structure from Fig. 5e, translating it and placing it then repeatedly into a volume. This volume was then rendered for visualization using the software package CHIMERA[51]. For processing, all steps were applied to the data at full pixel resolution of $4\ \mathrm{nm}$, for visualization and movie recording a reduced pixel size of $8\ \mathrm{nm}$ was used, applying an additional Gaussian Filter with weight 1.2 to reduce noise.

Supplementary References

50. Frank, J. *et al.* Spider and Web: Processing and Visualization of Images in 3D Electron Microscopy and Related Fields. *J Struct Biol.* **116**, 190-199 (1996).

51. Pettersen, E. F. *et al.* UCSF Chimera – A visualization system for exploratory research and analysis. *J Comput Chem.* **25**, 1605-1612 (2004).